UNCLASSIFIED

SECURITY CLASSIFICATION OF THIS PAGE (When Data Entered)

REPORT DOCUMENTATION PAGE		READ INSTRUCTIONS BEFORE COMPLETING FORM
1. REPORT NUMBER 18757.2-MA-H	2. GOVT ACCESSION NO. N/A	3. RECIPIENT'S CATALOG NUMBER N/A
4. TITLE (and Subtitle) Electromagnetic and Acoustic Resonance Scattering Theory		5. TYPE OF REPORT & PERIOD COVERED Reprint 6. PERFORMING ORG. REPORT NUMBER N/A
7. AUTHOR(s) H. Uberall, P. J. Moser, J. D. Murphy, A. Nagl, G. Igiri, J. V. Subrahmanyam, G. C. Gaunaurd, D. Brill, P. P. Delsanto, J. D. Alemar, E. Rosario		8. CONTRACT OR GRANT NUMBER(s) DAAG29 81 G 0016
9. PERFORMING ORGANIZATION NAME AND ADDRESS University of Puerto Rico Mayaguez, PR 00708		10. PROGRAM ELEMENT, PROJECT, TASK AREA & WORK UNIT NUMBERS N/A
11. CONTROLLING OFFICE NAME AND ADDRESS U. S. Army Research Office P. O. Box 12211 Research Triangle Park, NC 27709		12. REPORT DATE 1983 13. NUMBER OF PAGES 23
14. MONITORING AGENCY NAME & ADDRESS(if different from Controlling Office)		15. SECURITY CLASS. (of this report) Unclassified 15a. DECLASSIFICATION/DOWNGRADING SCHEDULE

16. DISTRIBUTION STATEMENT (of this Report)

Submitted for announcement only.

17. DISTRIBUTION STATEMENT (of the abstract entered in Block 20, if different from Report)

18. SUPPLEMENTARY NOTES

19. KEY WORDS (Continue on reverse side if necessary and identify by block number)

20. ABSTRACT (Continue on reverse side if necessary and identify by block number)

DD FORM 1 JAN 73 1473 EDITION OF 1 NOV 65 IS OBSOLETE

UNCLASSIFIED

SECURITY CLASSIFICATION OF THIS PAGE (When Data Entered)

WAVE MOTION 5 (1983) 307-329
NORTH-HOLLAND

ELECTROMAGNETIC AND ACOUSTIC RESONANCE SCATTERING THEORY

H. ÜBERALL*, P.J. MOSER†, J.D. MURPHY, A. NAGL, G. IGIRI, and J.V. SUBRAHMANYAM
Department of Physics, Catholic University, Washington, DC 20064, USA

G.C. GAUNAURD
Naval Surface Weapons Center, White Oak, Silver Spring, MD 20910, USA

D. BRILL‡
David Taylor Naval Ship Research and Development Center, Annapolis, MD 21402, USA

P.P. DELSANTO, J.D. ALEMAR, and E. ROSARIO
Department of Physics, University of Puerto Rico, Mayaguez, PR 00708, USA

Received 26 *February* 1982, *Revised* 15 *November* 1982

The excitation of the eigenfrequencies of finite radar or sonar targets, of inhomogeneities in elastic materials, of geological strata or of the entire earth by the impact of propagating waves (of electromagnetic or acoustic nature, or of ultrasonic, elastic, or seismic character, respectively) manifests itself in the appearance of poles in the resulting wave amplitudes, as described by the Resonance Scattering Theory (RST). In the complex frequency plane, these poles relate to the ringing of the scattering resonances. In the complex mode number plane, corresponding poles are connected with circumferential or creeping waves. An analytic relation between these two descriptions is indicated here, and a number of examples from the above-mentioned fields will be discussed. We introduce the concepts of '*Acoustic Spectroscopy*' and of '*Radar Spectroscopy*', respectively, by exhibiting the target's resonance frequency spectrum in a form familiar from atomic spectroscopy, in order to study the shifting and splitting of resonances 'levels' under changes of target shape, and to provide us with possible solutions for the 'inverse problem' (i.e., determination of target properties from echo properties – here, resonant echoes).

1. Introduction

Natural mechanic or electromagnetic oscillations of material objects take place at well-defined eigenfrequencies, determined by the constructive interference of internal and/or external surface waves of standing-wave type around the objects. The scattering of external scalar (acoustic) or vector (electromagnetic or elastic) waves by such objects at frequencies close to the natural eigenfrequencies exhibits a resonance character due to the excitation of the corresponding eigenvibrations [1]. In a modal description of scattering, the amplitude is governed by two variables, viz., the frequency variable and the mode number variable. A plot of the 'response surface' [2], i.e. of the scattering amplitude modulus in three dimensions plotted against these two variables, exhibits a series of parallel 'ripples' inclined to either axis. When intersecting this surface at a constant mode number, the ripples appear as frequency resonances, and intersecting at constant frequency, the same ripples lead to mode number resonances.

* Also Consultant, Naval Surface Weapons Center, White Oak, Silver Spring, MD 20910, USA
† Also at the Naval Research Laboratory, Washington, DC 20375, USA
‡ Also at the Department of Physics, US Naval Academy, Annapolis, MD 21402, USA

The mode number resonances are due to complex poles of the scattering amplitude known as 'Watson' [3] (or in nuclear physics, 'Regge' [4]) poles whose residues represent the mentioned surface waves (creeping waves), as previously studied by Franz [5]. The frequency resonances (known in nuclear physics as 'Breit–Wigner resonances' [6]) stem from poles in the complex frequency plane, originally studied on the basis of the 'Singularity Expansion Method' (SEM) by Baum [7]. In the latter context, they lead in the transient-field case to a Prony series-type superposition of decaying sinusoids which may be utilized to experimentally obtain the SEM pole positions for target characterization purposes. We have shown that the Prony series represents a mathematical concept which, when summed over appropriate subsets of complex-frequency poles, synthesizes individual surface waves which constitute the physical entities [8–10]. Examples will be shown of radar and acoustic, as well as elastic-wave and geophysical resonances, and possible uses of the resonance concept for the solution of the inverse scattering problem will be pointed out.

The inverse scattering concept refers to the determination of properties of the target from the characteristics of the scattering echo response [11–13]. It was shown previously that for targets of known (simple) geometry, target composition may be inferred from the location and the widths of resonances whose effects are carried by the scattered echo [14–21]. On the other hand, target *shape*, for a known target composition, may be inferred from the spectral scheme of the target resonances also, as shown by introducing the concepts of '*Acoustic Spectroscopy*' [22], or of '*Radar Spectroscopy*' [23], respectively. Here, we plot the eigenfrequency spectra of acoustic or of radar targets in a way familiar from atomic spectroscopy, and study the shifting and splitting of the resonance 'levels' under changes of target shape, thus assessing the sensitivity of the mechanical or electromagnetic eigenfrequency spectra of targets to their shapes, which offers the possibility of determining target shape from a spectral analysis of the resonant echoes.

2. SEM poles and surface waves in radar scattering

We shall first deal with resonance effects in steady-state radar-scattering. For the plane electromagnetic wave incident upon the north pole of a spherical scatterer, the scattered far field is given in spherical coordinates by [24]:

$$\boldsymbol{E}_{sc} = (E_0/r)\, e^{ik_0 r - i\omega t}\{\hat{\varepsilon}_\theta S_1(\theta)\cos\phi - \hat{\varepsilon}_\phi S_2(\theta)\sin\phi\}, \tag{1a}$$

where $k_0 = \omega/c$ is the wave number in vacuum. The polarization functions $S_{1,2}$ are, e.g.

$$S_1(\theta) = -i\sum_{n=1}^{\infty}(-1)^n \frac{2n+1}{n(n+1)}\left\{a_n \frac{P_n^1(\cos\theta)}{\sin\theta} - b_n \frac{dP_n^1(\cos\theta)}{d\theta}\right\} \tag{1b}$$

with 'Mie coefficients'

$$a_n = -\frac{xj_n(x) - iZ_n[xj_n(x)]'}{xh_n^{(1)}(x) - iZ_n[xh_n^{(1)}(x)]'}, \tag{1c}$$

$$b_n = -\frac{xj_n(x) - iY_n[xj_n(x)]'}{xh_n^{(1)}(x) - iY_n[xh_n^{(1)}(x)]'}, \tag{1d}$$

where $x = k_0 a$ with a being the radius of the sphere.

Reference [24] gives expressions for the modal impedances Z_n and admittances Y_n of variously layered spheres; for a homogeneous dielectric sphere of permeability $\mu = 1$, one has, e.g.

$$Z_n = -\mathrm{i}\frac{k_0}{k}\frac{x_1 j_n(x_1)}{[x_1 j_n(x_1)]'}, \tag{2a}$$

$$Y_n = -\mathrm{i}\frac{k}{k_0}\frac{x_1 j_n(x_1)}{[x_1 j_n(x_1)]'}, \tag{2b}$$

where $x_1 = ka$, $k = \omega/c_1$, c_1 being the speed of light in the dielectric. For a perfectly conducting sphere, one has $Z_n = 0$, $Y_n = \infty$.

Complex eigenfrequencies of the spherical target are obtained as the roots of the denominators of (1c) ('TE modes') or (1d) ('TM modes'). However, for penetrable targets such as dielectric spheres, or conducting spheres with dielectric coating, the resonances in the scattered echoes as functions of frequency are sharp and narrow, as can be seen in Fig. 1 where the radar cross section

$$\sigma = \frac{4\pi}{k_0^2}\left|\sum_{n=1}^{\infty}(-1)^n(n+\tfrac{1}{2})(a_n - b_n)\right|^2 \tag{3}$$

of a dielectrically-coated conducting sphere (outer radius a) is plotted vs. $k_0 a$ for $k_0 a = 37$–41. Accordingly, the imaginary parts of the denominators are small, and the real resonance frequencies x_n^{TE}, x_n^{TM}

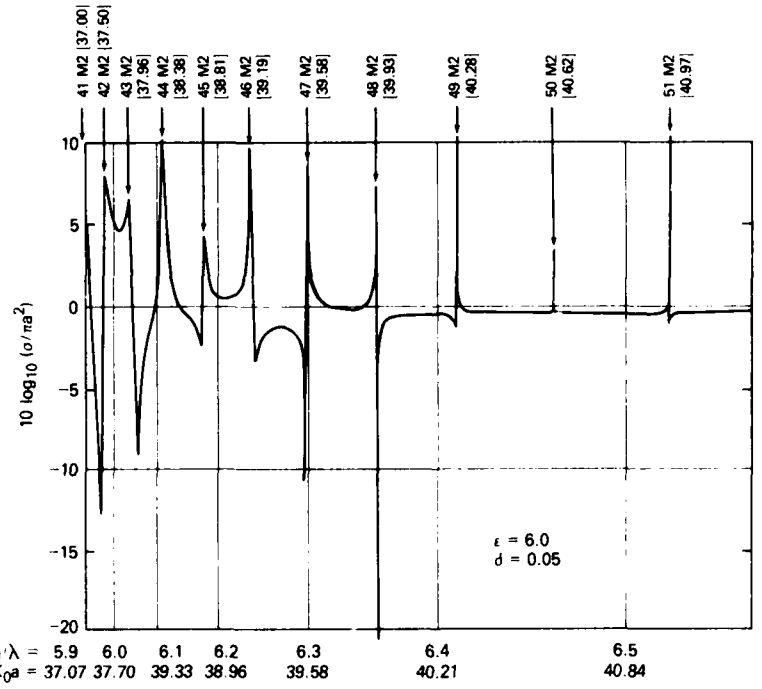

Fig. 1. Radar cross section for a conducting sphere coated with a dielectric of dielectric constant $\epsilon = 6$, relative thickness $\delta = 0.05$, and an outer radius a, plotted vs. $x = k_0 a = 2\pi a/\lambda$ (from [25]).

are found as the solutions of

$$1/(\mathrm{i}Z_n) = \mathrm{Re}\{[xh_n^{(1)}(x)]'/[xh_n^{(1)}(x)]\}, \quad \text{TE modes,} \tag{4a}$$

$$\mathrm{i}Y_n = \mathrm{Re}\{[xh_n^{(1)}(x)]/[xh_n^{(1)}(x)]'\}, \quad \text{TM modes,} \tag{4b}$$

with multiple roots labeled by $l = 1, 2, 3 \ldots$.

The expressions of (2) for the dielectric sphere are meromorphic functions (which in nuclear physics are known as Wigner's R matrix or 'derivative matrix' [6]) that may be represented by Mittag–Leffler series, e.g. for TM modes [25]:

$$1/(\mathrm{i}Y_n) = \frac{k_0}{k} \sum_{l=-\infty}^{\infty} \frac{1}{x - \tilde{x}_{nl}}, \tag{5a}$$

the (real) pole positions being given by the expressions

$$\tilde{x}_{nl} = z_{nl}(c_1/c) \tag{5b}$$

where z_{nl} are the zeros of $j_n(z)$, their multiplicity being labelled by l.

We may introduce the 'S-function' $S_n^{\mathrm{TM}} = 1 + 2b_n$ and find

$$S_n^{\mathrm{TM}} = S_n^{(0)\mathrm{TH}} \frac{\mathrm{i}Y_n - z_n^{(2)}}{\mathrm{i}Y_n - z_n^{(1)}}, \tag{6a}$$

where

$$z_n^{(i)} = \frac{h_n^{(i)}(x)}{[xh_n^{(i)}(x)]'} \equiv \sigma_n(x) \mp \mathrm{i}\pi_n(x) \quad (i = 1, 2), \tag{6b}$$

the quantity

$$S_n^{(0)\mathrm{TM}} = -\frac{[xh_n^{(2)}(x)]'}{[xh_n^{(1)}(x)]'} \equiv \mathrm{e}^{2\mathrm{i}\zeta_n} \tag{6c}$$

being the S-function of a conducting sphere. Accordingly, the S-function

$$S_n^{\mathrm{TM}} = S_n^{(0)TM} \frac{1 - (\sigma_n + \mathrm{i}\pi_n)(\mathrm{i}Y_n)^{-1}}{1 - (\sigma_n - \mathrm{i}\pi_n)(\mathrm{i}Y_n)^{-1}}, \tag{6d}$$

with (5a) being used for $(\mathrm{i}Y_n)^{-1}$, exhibits the singularity structure of the scattering amplitude. The S-function thus has two kinds of TM poles, those given by the zeros of $[xh_n^{(1)}(x)]'$ corresponding to the (broad) resonances of electromagnetic waves propagating over the exterior of the sphere, and those given by the roots of (4b) corresponding to internal-wave resonances, only these being sharp and narrow.

For the latter case, one may consider one resonance at a time in (6d), and thus obtain the 'one-level approximation' [25, 26]

$$S_n^{\mathrm{TM}} \cong \sum_l S_n^{(0)\mathrm{TM}} \frac{x - x_{nl}^{\mathrm{TM}} - (\mathrm{i}/2)\Gamma_{nl}^{\mathrm{TM}}}{x - x_{nl}^{\mathrm{TM}} + (\mathrm{i}/2)\Gamma_{nl}^{\mathrm{TM}}}, \tag{7a}$$

the so-called Breit–Wigner form of the S-function [6], in which the resonance frequencies are

$$x_{nl}^{\mathrm{TM}} = \tilde{x}_{nl}^{\mathrm{TM}} - (k_0/k)\sigma_n(\tilde{x}_{nl}^{\mathrm{TM}}), \tag{7b}$$

and the resonance widths are

$$\Gamma_{nl}^{\mathrm{TM}} = 2(k_0/k)\pi_n(\tilde{x}_{nl}^{\mathrm{TM}}). \tag{7c}$$

Returning to the Mie coefficients, one has, e.g.,

$$b_n = \mathrm{i}\left\{\sum_l S_n^{(0)\mathrm{TM}}(x_{nl}^{\mathrm{TM}})\frac{-(1/2)\Gamma_{nl}^{\mathrm{TM}}}{x - x_{nl}^{\mathrm{TM}} + (\mathrm{i}/2)\Gamma_{nl}^{\mathrm{TM}}} + \mathrm{e}^{\mathrm{i}\xi_n}\sin\xi_n\right\} \tag{7d}$$

where the first term represents a series of internal resonances, superimposed upon and interfering with the second term which consists of a relatively smooth background containing only quite broad resonances corresponding to those of a conducting sphere, together with a specularly reflected amplitude [5].

The resonance frequencies of (7a) or (7d) are thus given by the (complex) pole positions

$$\hat{x}_{nl} = x_n - (\mathrm{i}/2)\Gamma_{nl} \tag{8}$$

representing the 'SEM poles' [7] in the complex frequency plane. For (physical) real frequencies x, however, the expressions of (7a), (7d) will pass over resonance peaks of finite height as x is varied, which appear as the foothills of distant, very (in fact, infinitely) high mountain peaks located at the poles themselves [27]. For the real-frequency case, one may instead look for poles in the (complex) mode number variable n, by expanding [28]

$$x_{nl} \cong x_{n_l l} - (n - n_l)x'_{n_l l} + \cdots \quad , \tag{9a}$$

and with n_l so chosen that $x_{n_l l} = x$. This brings the denominators of (7a), (7d) into the form $n - \hat{n}_l$, where

$$\hat{n}_l = n_l + (\mathrm{i}/2)\hat{\Gamma}_{n_l l} \tag{9b}$$

with

$$\hat{\Gamma}_{n_l l} = \Gamma_{n_l l}/x'_{n_l l}. \tag{9c}$$

Accordingly,

$$S_n \cong \sum_l S_n^{(0)}\frac{n - \hat{n}_l^*}{n - \hat{n}_l}, \tag{9d}$$

and $\hat{n}_l$ of (9b) gives the position of 'Watson poles' (or 'Regge poles') in the complex n (mode number) plane.

The above-described mathematical steps leading from (7a) or (7d) to (9d) may be represented geometrically as follows. We show the modulus of the resonance part of (7d) in Fig. 2 (the figure actually depicts the analogous case of the amplitude of compressional elastic waves scattered from a fluid-filled sphere [29]) as a three dimensional plot, representing the 'response surface' above a plane with one axis being the frequency, the other axis the mode number n. The response surface shows a series of parallel ripples inclined with either axis. If these are intersected at a constant value of n, there result the SEM resonances vs. frequency; but if the ripples are intersected at constant frequency, resonances in n are obtained which are a result of the Regge poles.

In Fig. 3, we plot the modulus of the resonance portion of b_n, (7d), versus frequency for $n = 1, 4, 7$ and 10 for the case of a dielectrically coated conducting sphere.

The corresponding resonance curves are the first mentioned intersections representing the SEM-pole resonances; they are seen to contain families of resonances whose members (termed 'Regge recurrences') shift to higher frequencies with increasing n due to the inclination of the mentioned ripples with either axis. Each family corresponds to a surface wave, since asymptotically,

$$P_\nu^1(\cos\theta) \propto \cos[(\nu + \tfrac{1}{2})\theta + \tfrac{1}{4}\pi] \tag{10a}$$

so that (1) contain residue factors from the Regge poles which have the form

$$\exp \mathrm{i}\{\pm(\hat{n}_l + \tfrac{1}{2})\theta \pm \tfrac{1}{4}\pi - \omega t\}. \tag{10b}$$

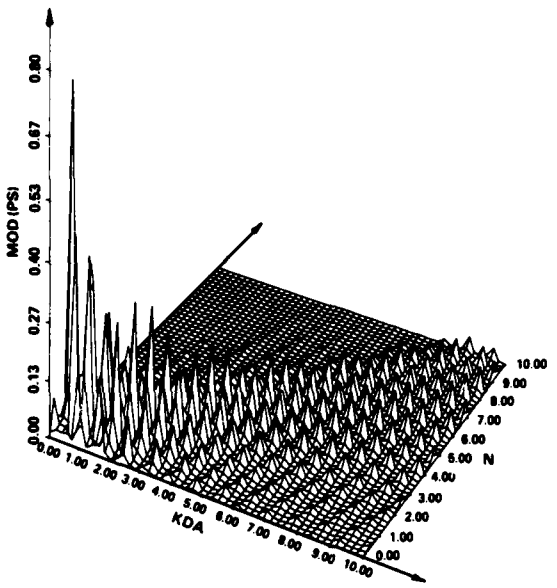

Fig. 2. Response surface of the resonance amplitude for compressional-wave scattering (with mode conversion into shear waves) from a water-filled spherical cavity in aluminum (from [29]).

This represents a circumferential (surface) wave with a linear propagation constant $\mathrm{Re}(\hat{n}_l+\frac{1}{2})/a$, i.e. a phase velocity

$$c_l(x)=xc/(n_l+\tfrac{1}{2}) \tag{11a}$$

for the lth surface wave, a wavelength

$$\lambda_l(x)=2\pi a/(n_l+\tfrac{1}{2}) \tag{11b}$$

such that resonance ($n_l=n$), $n+\frac{1}{2}$ wavelengths fit the circumference, and an attenuation $\exp(-\theta/\theta_l)$ where

$$\theta_l=2/\hat{\Gamma}_{n,l} \tag{11c}$$

which is due to radiation. Figure 4 shows 'dispersion curves' $c_l(x)$ vs. x for the TM-mode surface waves $l=1$–4 on the coated sphere of Fig. 3 (solid curves), and on a dielectric sphere ($\varepsilon=6$) of equal radius (dashed curves). The above analysis has thus led to a conceptual, as well as analytic, connection between SEM poles on one hand, and surface waves (represented by Regge poles) on the other.

3. SEM poles and surface waves in acoustic scattering

The poles in acoustic scattering amplitudes can be treated in an entirely analogous fashion. The total (incident and scattered) pressure amplitude in a fluid medium ambient to a solid sphere may be written as [1]

$$p=e^{-i\omega t}\sum_{n=0}^{\infty} i^n(2n+1)\{j_n(kr)+(B_n/D_n)h_n^{(1)}(kr)\}P_n(\cos\theta), \tag{12}$$

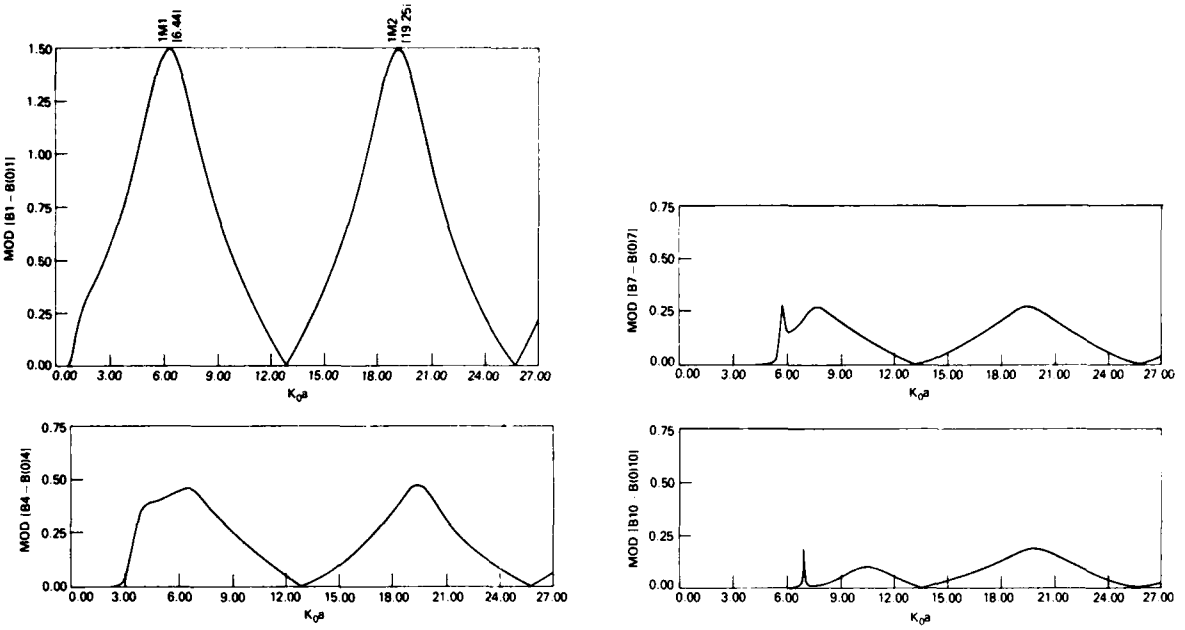

Fig. 3. Modulus of the resonance portion of b_n for a dielectrically coated conducting sphere ($\epsilon = 6$, $\delta = 0.1$), for $n = 1$, 4, 7 and 10 (from [25]).

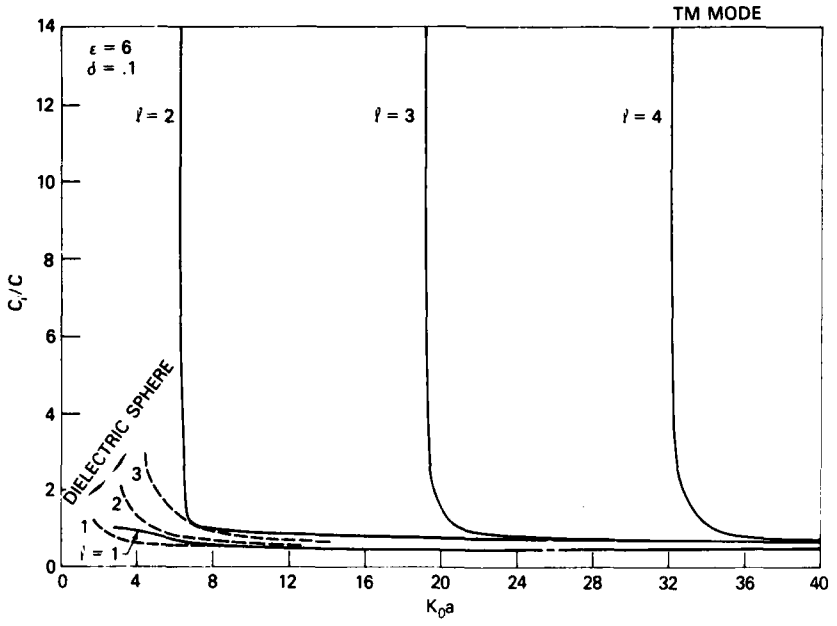

Fig. 4. Dispersion curves $c_l(x)$ of surface waves labeled $l = 1$–4 on a dielectrically coated conducting sphere ($\epsilon = 6$, $\delta = 0.1$), and for surface waves $l = 1$–3 on a dielectric sphere ($\epsilon = 6$) of equal radius (from [25]).

where B_n and D_n may be explicitly given as 3×3 determinants, containing spherical Hankel and Bessel functions whose arguments are $x \equiv ka$ ($k = \omega/c$, c being the ambient sound velocity), and Bessel functions with arguments $k_d a$ and $k_s a$ where k_d, k_s are the propagation constants of bulk dilatational and shear waves, respectively, in the sphere material. The SEM poles are the solutions of

$$D_n(x) = 0; \tag{13a}$$

they are the complex eigenfrequencies x_{nl} which we label by $l = 1, 2, 3 \ldots$. The Regge poles are the solutions of

$$D_\nu(x) = 0 \tag{13b}$$

with real x, i.e., they are the complex pole values $\nu_l(x)$ which as in Section 2, represent the propagation constant of the lth surface wave.

We have solved (13a) numerically for a tungsten-carbide sphere (characterized by a density $\rho_s = 13.80\ \mathrm{g/cm^3}$ and by bulk wave speeds $c_d = 6.860\times10^5$ cm/s and $c_s = 4.185\times10^5$ cm/s) immersed in water ($\rho = 1\ \mathrm{g/cm^3}$, $c = 1.4760\times10^5$ cm/s). The SEM poles $\hat{x}_{nl}$ in the complex x-plane are shown in Fig. 5; pole families corresponding to a given surface wave are connected by solid lines. Bollig and Langenberg [27] give analogous results for an aluminum sphere.

We distinguish here the pole series corresponding to the first ($l = 1$) surface wave, which has an entirely different appearance from those of the other surface waves; in particular, it has much larger imaginary parts so that this surface wave is more highly attenuated. This wave has been termed the 'Rayleigh wave' [30], since in the limit of infinite cylinder radius, it goes over into the well-known Rayleigh wave on the flat boundary of a solid half-space. The other surface waves ($l \geq 2$), are referred to as the 'Whispering–Gallery Waves'.

Using (11a) at the resonance frequencies, Fig. 5 can be made to yield the dispersion curves of Rayleigh and Whispering–Gallery waves. A few of these are shown in Fig. 6, where the Rayleigh-wave phase

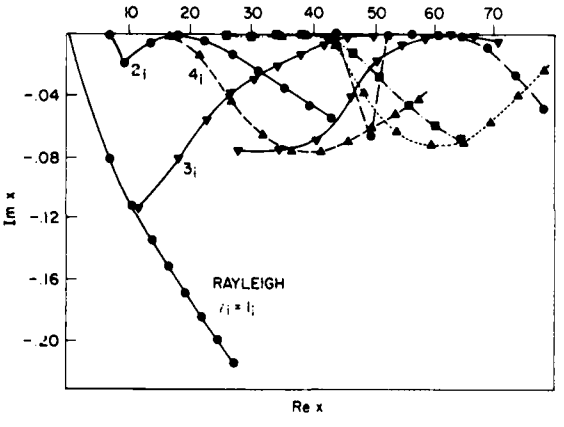

Fig. 5 SEM poles in the complex frequency plane for a tungsten-carbide sphere immersed in water (from [30]). Pole layers of these internal surface waves are labeled by l_i.

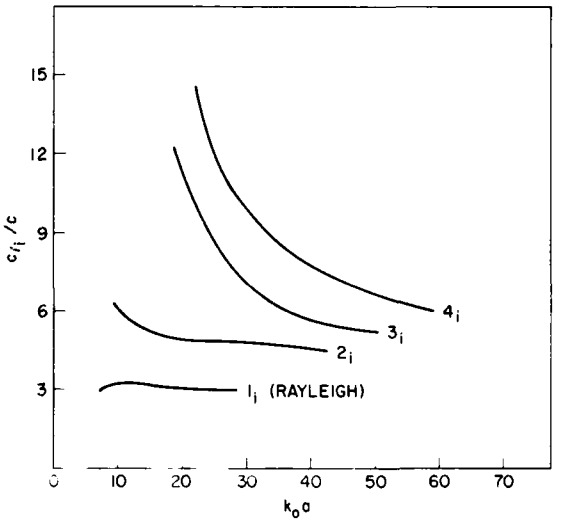

Fig. 6. Dispersion curves for (internal) Rayleigh and Whispering–Gallery surface waves on a tungsten-carbide sphere (labeled by l_i).

velocity is seen to start from zero at low frequency, while the Whispering–Gallery waves only exist above an individual cutoff frequency at which their phase velocity decreases down from infinity.

The SEM poles shown in Fig. 5 correspond to 'internal' surface waves that propagate with speeds comparable to the bulk velocities of the target material. In addition, there also exist external, or Franz-type [5] 'creeping' waves that propagate in the ambient medium around the scatterer, with speeds comparable to the corresponding sound speed. Their poles cannot be shown in Fig. 5 because their imaginary parts are of order unity or larger; hence they are much more highly damped than the internal surface waves.

Apart from spheres, acoustic SEM poles can also be discussed easily for infinite-cylindrical targets [31]. If a plane wave is incident on such a cylinder, its wave vector making an angle γ with the z-axis (i.e., the cylinder axis), so that the components of the propagation vector $k = \omega/c$ are $k_x = k \sin\gamma$, $k_y = k\cos\gamma$, one then has a scattered solution

$$p_s = e^{ik_z z - i\omega t} \sum_{n=0}^{\infty} (2-\delta_{n0}) i^n T_n H_n^{(1)}(k_x r)\cos n\theta, \tag{14a}$$

with an S- function $S_n \equiv 2T_n + 1$ given by

$$S_n = S_n' \frac{L_n^{-1} - [z_n^{(2)}(k_x a)]^{-1}}{L_n^{-1} - [z_n^{(1)}(k_x a)]^{-1}}, \tag{14b}$$

where

$$z_n^{(i)}(x) = \frac{xH_n^{(i)\prime}(x)}{H_n^{(i)}(x)} \quad (i = 1, 2), \tag{14c}$$

and where

$$S_n' = -\frac{H_n^{(2)\prime}(k_x a)}{H_n^{(1)\prime}(k_x a)} \tag{14d}$$

is the S-function of a rigid impenetrable cylinder. For the case of a fluid cylinder of density ρ' and wave number k', one has, e.g.,

$$L_n = \frac{\rho}{\rho'} \frac{k_x' a J_n'(k_x' a)}{J_n(k_x' a)} \tag{14e}$$

(ρ being the density of the ambient fluid). S_n and T_n may be represented in resonance form as in (7a), (7d), and the internal surface waves derived accordingly. They are found to propagate over the cylinder surface along helical paths with pitch angles (with the z-axis)

$$\gamma_l = \tan^{-1}(n_l/ak_z), \tag{15a}$$

and with phase velocities

$$c_l = \frac{c}{\{\cos^2\gamma + (n_l/ka)^2\}^{1/2}}, \tag{15b}$$

(15b) being the cylinder-equivalent of the spherical surface wave speed of (11a).

For impenentrable (e.g., rigid) cylinders ($\rho' \gg \rho$), the resonances in (14b), and hence the internal resonances, are absent and only the resonances due to external creeping waves exist. From (14d), these

are determined by the roots of

$$H_n^{(1)'}(k_x a) = 0, \tag{16a}$$

which for real integer n represent the external SEM poles in the $k_x a$ plane. However, (16a) has been solved by Franz [5] for real $k_x a$ in terms of the Regge poles in the complex n-plane, with the result

$$\hat{n}_l(x) = x + (x/6)^{1/3}\, e^{i\pi/3} q_l + \cdots \quad (x \equiv k_x a), \tag{16b}$$

where $q_l = 1.469354$ etc. This gives directly the propagation constant of the creeping waves, whose dispersion curves are thus found as

$$c_l = \frac{c}{1 = \dfrac{q_l}{2.6^{1/3}}\left(\dfrac{\sin^2\gamma}{ka}\right)^{2/3} + \cdots} \tag{16c}$$

for the phase velocities, and

$$c_l^{gp} = \frac{c}{1 + \dfrac{q_l}{6^{4/3}}\left(\dfrac{\sin^2\gamma}{ka}\right)^{2/3} + \cdots} \tag{ }$$

for the group velocities.

As discussed in [31], very interesting refraction effects occur upon the generation of surface waves by the incident wave since $\gamma_l \neq \gamma$. They consist in a change of propagation direction, either in the axial direction for Franz waves and for internal surface waves with $c_l \leq c$, or in the radial direction for internal surface waves with $c_l \geq c$.

4. Surface waves on the earth

The example of seismic waves represents a case of surface waves that are not generated by the scattering of plane waves, but by the action of point sources (e.g., depth charges, or earthquakes). Apart from this, the theory is exactly the same as that described in Section 2. In particular, the phase and group velocities of the seismic surface waves are given by

$$c_l(x) = \frac{xc}{n_l + \frac{1}{2}} \tag{17a}$$

and

$$c_l^{gp}(x) = \frac{c}{dn_l/dx} \tag{17b}$$

respectively, where $x = \omega a/c$, a being the earth radius, ω the circular frequency of the waves, and c a convenient reference speed which actually drops out in (17). These equations may be evaluated at the known eigenfrequencies of the earth x_{nl}, at which one has $n_l \to n$ (integer).

The earth may undergo two types of eigenvibrations, namely, spheroidal and toroidal (torsional) ones. Surface displacement components (u, v, w) in the (r, θ, ϕ) directions for a spherical, radially stratified

earth may be represented as [32]

$$u = \sum_{n,m} U_n(r,\omega)\, Y_n^m(\theta,\phi) \tag{18a}$$

$$v = \sum_{n,m} \left\{ \Psi_n(r,\omega) \frac{\partial Y_n^m}{\partial \theta} + \frac{\Omega_n(r,\omega)}{\sin\theta} \frac{\partial Y_n^m}{\partial \phi} \right\}, \tag{18b}$$

$$w = \sum_{n,m} \left\{ \frac{\Psi_n(r,\omega)}{\sin\theta} \frac{\partial Y_n^m}{\partial \phi} - \Omega_n(r,\omega) \frac{\partial Y_n^m}{\partial \theta} \right\}, \tag{18c}$$

and U_n, Ψ_n represent spheroidal modes of vibration which are uncoupled from Ω_n, the toroidal vibration modes.

Gilbert and Dziewonski [33] have empirically determined a total of 1064 eigenfrequencies x_{nl} of the earth, both spheroidal and toroidal, essentially by Fourier-analyzing observed earthquake shocks. Using these data, we obtain e.g. the phase velocities of spheroidal (Fig. 7) and toroidal (Fig. 8) seismic surface waves [34], plotted vs. the period $\tau = 2\pi/\omega$, as solid lines connecting the data (points). These dispersion curves are remarkably similar to those of Fig. 4 or 6 except for now being plotted against the inverse frequency variable. The curves are labelled by the order $l = 0, 1, 2 \ldots$ of the surface waves, and are compared with the theoretically predicted phase velocities (broken curves or open circles) of the so-called Gutenberg–Bullen A′ model [35] which consists of a solid mantle overlying a fluid core at a depth of 2900 km, with an inner core at 5200 km.

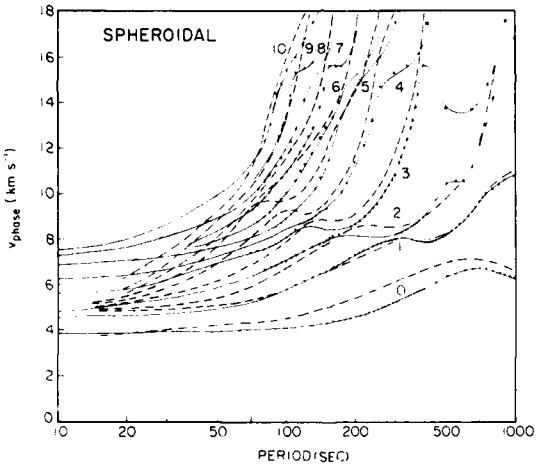

Fig. 7. Dispersion curves for the phase velocities of spheroidal surface waves $l = 0$–10 (as labeled), obtained from the empirical eigenfrequencies of the earth (solid curves and data points), and of surface waves $l = 0$–9 from the Gutenberg–Bullen A′ earth model (dashed curves), plotted vs. the period (from [34]).

In Fig. 7, one observes a transition region at $c_l \sim 8$ km/s at which successive surface waves form the dispersion curve of a 'pseudomode', attributed [35] to the existence of a Stoneley wave on the core-mantle boundary which affects only spheroidal modes. Our analysis obtains a second transition region at $c_l \sim 15$ km/s which is not predicted by the Gutenberg–Bullen model.

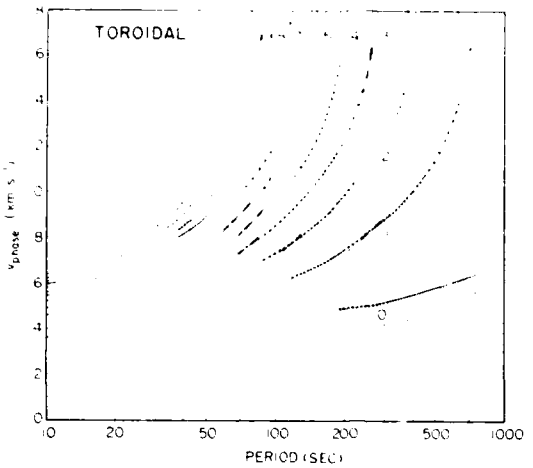

Fig. 8. Similar to Fig. 7, for toroidal surface waves (from [34]).

5. SEM poles and creeping waves (transients)

The effect of SEM poles on transients, as well as the case of transient creeping waves, will now be discussed using the example of a perfectly conducting sphere, and restricting ourselves to TM modes. The corresponding TM part of the first polarization function, (1b), is thus

$$S_1^{\mathrm{TM}}(\theta) = -\mathrm{i} \sum_{n=1}^{\infty} (-1)^n \frac{2n+1}{n(n+1)} \frac{[xj_n(x)]'}{[xh_n^{(1)}(x)]'} \frac{\mathrm{d}P_n^1(\cos\theta)}{\mathrm{d}\theta}. \tag{19}$$

The complex-frequency SEM poles are given by the complex zeros of $[xh_n^{(1)}(x)]'$ which we denote again by $\hat{x}_{nl}$. These zeros were obtained by us numerically and, in Fig. 9 are plotted in the plane of the variable $sa/c = -\mathrm{i}x$, rather than of x (in which the figure would appear rotated counter clockwise by 90°), since it is customary in SEM theory to represent the complex poles in the plane of the Laplace variable s. The dashed lines link the poles according to mode number n. When the poles are grouped in (non-symmetric) 'layers', however (solid lines in Fig. 9, labeled by l), then each layer will synthesize one (the lth) creeping wave [8]. The present, correct system of layering [9] differs from that of [8], and can be rigorously arrived at as follows. The spherical Watson (Regge) zeros of $[xh_x^{(1)}(x)]'$ in the n-variable are given asymptotically by [5]:

$$\hat{n}_l(x) + \tfrac{1}{2} \cong x + (x/6)^{1/3} \mathrm{e}^{\mathrm{i}\pi/3} q_l + \cdots, \tag{20a}$$

with q_l the same as quoted after Eq. (16b). The label l determines here the lth creeping wave, $\hat{n}_l + \frac{1}{2}$ being its propagation constant, *c.f.* (10b).

Equation (20a) may be inverted, by replacing $\hat{n}_l \to n$ and solving for $x = \hat{x}_{nl}$, in order to obtain an asymptotic expression for the SEM pole positions $\hat{x}_{nl}$:

$$\hat{x}_{nl} \cong n + \tfrac{1}{2} - (n+\tfrac{1}{2})^{1/3} 6^{-1/3} \mathrm{e}^{\mathrm{i}\pi/3} q_l + \cdots. \tag{20b}$$

When this expression is plotted in the diagram of Fig. 9, the asymptotic pole positions of (20b) agree quite closely with the exact (numerical) pole positions shown in Fig. 9. However, while the numerical pole calculation only furnishes the n-value of each pole, use of (20b) in addition determines its l-value, i.e., it tells us which poles belong to a layer of given l and thus, give rise to the lth creeping wave. The

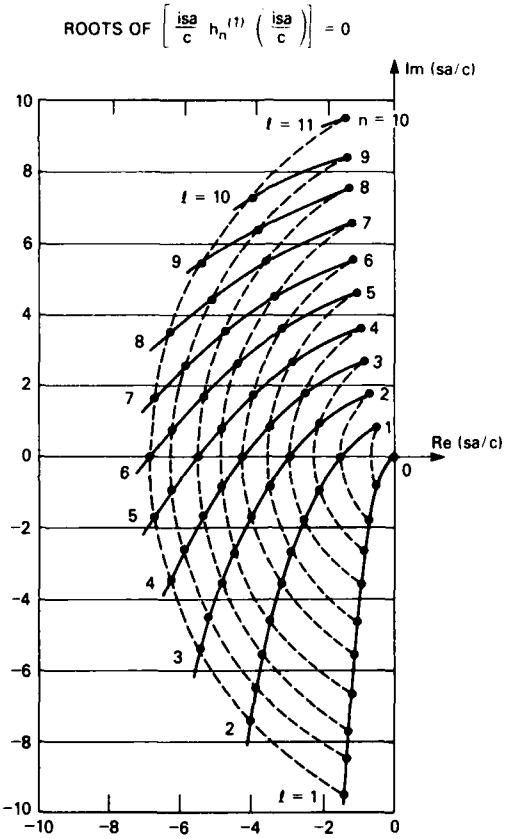

Fig. 9. Poles of TM modes of oscillations of a conducting sphere in the complex frequency plane ($\omega = is$). Dashed curves connect zeros of given n; solid curves connect zeros of given l whose residues synthesize the lth creeping wave (from [9]).

asymptotic expression of (20b) thus serves to uniquely and rigorously establish the correct connection between SEM poles and creeping waves.

Note that the (solid-curve) pole layers in Fig. 9 that belong to the lth creeping wave are non-symmetric about the horizontal axis. The statement of [7], namely that for reasons of the overall reality of the field solutions to the scattering problem, the poles have to be symmetrical about this axis, is not contradicted thereby since inspection of Fig. 9 shows that the *individual* poles *are* located symmetrically above and below the horizontal. Only their *ordering* into creeping-wave layers is non-symmetric. Evidently, individual creeping waves may be described by complex fields, but the total field obtained by summing over all creeping waves is real. Note also that for the case of an infinite cylinder, the individual SEM poles were found [36] to be symmetrical again, but here the situation is more complicated since $H_n^{(1)}(x)$ has a branch cut running from the origin of the s-plane horizontally to the left, dividing the upper and lower s-plane into two different sheets of which only those sheets containing symmetrical poles appear to be the physical ones. No branch cut, and thus only one single sheet, exists for the present case of the sphere.

The SEM poles can be exhibited in the denominator of (19) by Taylor-expanding $[xh_n^{(1)}(x)]'$ about its zeros. Calling

$$T_1(\theta) = (1/kr)\, e^{i(kr-\omega t)} S_1^{TM}(\theta), \tag{21a}$$

one obtains

$$T_1(\theta) = \frac{e^{i(kr-\omega t)}}{ir/a} \sum_{l=1}^{\infty} \sum_{n=1}^{\infty} \frac{(-1)^n}{x-\hat{x}_{nl}} \frac{n+\frac{1}{2}}{\hat{x}_{nl}} \frac{[\hat{x}_{nl} j_n(\hat{x}_{nl})]'}{[\hat{x}_{nl} h_n^{(1)}(\hat{x}_{nl})]'} \left\{ \frac{2}{n(n+1)} \frac{dP_n^1(\cos\theta)}{d\theta} \right\}; \tag{21b}$$

for backscattering ($\theta = 0$), the last factor becomes unity. The first factor after the summation sign represents the SEM poles. Proceeding now to the transient case, we assume an incident δ-pulse, $\delta(z + ct)$, and with a dimensionless time variable $\tau = (ct - r)/a$ we obtain

$$T_1(\theta, \tau) = \sum_{l=1}^{\infty} T_1^{(l)}(\theta, \tau) \tag{21c}$$

where for $\theta = 0$:

$$T_1^{(l)}(0, \tau) = -\frac{1}{r} \sum_{n=1}^{\infty} (-1)^n \frac{n+\frac{1}{2}}{\hat{x}_{nl}} \frac{[\hat{x}_{nl} j_n(\hat{x}_{nl})]'}{[\hat{x}_{nl} h_n^{(1)}(\hat{x}_{nl})]'} e^{-i\hat{x}_{nl}\tau}. \tag{21d}$$

In view of (8), this expression has the standard SEM form for transient radar echoes, i.e., it consists of a superposition of damped sinusoids (sometimes referred to as a Prony series). While, however, SEM theory applied this expression to (21c) for $T_1(\theta, \tau)$ as a whole, we consider in (21d) separately the terms $T_1^{(l)}(\theta, \tau)$, i.e., a Prony *sub*-series summed only over poles in one layer of given l, the reason being that this subseries synthesizes the lth creeping wave.

In Fig. 10 we plot on an arbitrary scale the quantity $X(\tau) = r \operatorname{Re} T_1^{(1)}(0, \tau)$, i.e., the backscattering amplitude for the first creeping wave. It has here been evaluated [37] using the asymptotic expressions for the poles of (20b). While the individual damped sinusoids in (21d) are quite large numerically especially near $\tau = 0$, they all cancel in the sum except near $\tau = \pi$, 3π, etc., which are the correct arrival times of a multiply-circumnavigating creeping wave with velocity c. The exact arrival times, however, are determined by the group velocities of the creeping waves. Using the fact that asymptotically, $P_n^1(\cos\theta) \propto \cos[(n+\frac{1}{2})\theta - (\pi/4)]$, and inserting this and (20b) in (21d), one may evaluate the ensuing sum by the method of stationary phase. It can be shown that the ratio of spherical cylinder functions asymptotically has no exponential behavior. If to lowest order, $\hat{x}_{nl}$ is approximated by $n+\frac{1}{2}$, the sum has stationary phase for $\tau = (2N+1)\pi$ where $N = 0, 1, 2, \ldots$, proving the multiple (N-fold) circumnavigations. To higher order, the phase ϕ_{nl} of (21d), i.e.,

$$\phi_{nl} = (2N+1)\pi n - x_{nl}\tau \tag{22}$$

(with $x_{nl} = \operatorname{Re} \hat{x}_{nl}$), must be stationary, i.e., its derivative with respect to n must vanish. Noting that phase and group velocities of the creeping waves are given by [8]

$$c_l(x)/c = x/\operatorname{Re}[\hat{n}_l(x) + \tfrac{1}{2}], \tag{23a}$$

$$c_l^{gp}(x)/c = 1/\operatorname{Re}[d\hat{n}_l(x)/dx], \tag{23b}$$

one recognizes using (20a) that the stationary-phase condition on (22) leads to the dimensionless arrival time of the backscattered pulses:

$$\tau_{arr} = (2N+1)\pi/(c_l^{gp}/c), \tag{23c}$$

or, going back to actual time:

$$t_{arr} = (2N+1)\pi a/c_l^{gp}, \tag{23d}$$

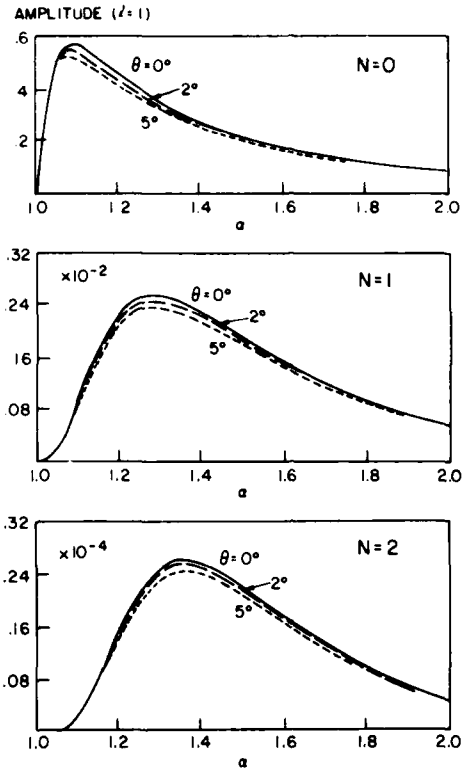

Fig. 10. Pulses of $l = 1$ (TM) creeping wave in the scattering amplitude $-r$ Re $T_1^{(1)}(0, \tau)$ as synthesized by the appropriate Prony subseries, evaluated by the stationary-phase method (from [37]), and plotted vs. a new time variable $\alpha \equiv \tau/[(2N+1)\pi + \theta]$, as measured from the individual pulse arrival times at $\alpha = 1$ onward.

showing that the creeping-wave pulses propagate with the group velocity. The actual pulse shapes of the first TM creeping wave, shown in Fig. 10, are those obtained at or shortly after ($\leq 5°$) one-half ($N = 0$, top), $1\frac{1}{2}$ ($N = 1$, center) and $2\frac{1}{2}$ ($N = 2$, bottom) circumnavigations of the sphere, by replacing the sum over n in (21d) by an integral which was evaluated using the stationary phase method. The flowing-apart of the pulse due to dispersion, and its attenuation in the course of the multiple circumnavigations, due to radiation, is evident.

6. Analysis of transient creeping wave experiments

Experiments on the scattering of short electromagnetic pulses from conducting spheres and cylinders have been carried out by B.Z. Hollmann of the Naval Surface Weapons Laboratory, Dahlgren, VA, USA [38]. The experimental arrangement consisted of a conducting ground plane with a vertical conical transmitter (S) in the center whose tip touched the ground plane; its length was 13 ft 9 in. and its half opening angle 5.29 degrees, and it generated a near-plane wave field with a vertical electric vector. The receiver antenna (R), a half TEM horn, rested on the ground plane, as did the targets: a hemisphere as well as a lying-down half-cylinder whose mirror image at the plane completed them to a full sphere and cylinder, and an upright cylinder whose length was doubled by the mirror image.

The transmitter generated a 1-ns pulse with a smaller negative overshoot of 1.5 ns duration. It could be represented by

$$p_{\text{inc}}(t) = \int_{-\infty}^{\infty} G(\omega) \exp(-i\omega t)\, d\omega, \tag{24a}$$

with a spectrum $G(\omega)$ determined from the experimental pulse shape by Fourier inversion. We shall here discuss the experimental case of the half-cylinder lying flat on the ground plane, shown in top view in Fig. 11. The echo pulses then consisted, in their order of arrival time, of a specularly reflected pulse (1), two coinciding pulses (2,2') reflected from the cylinder edge, and a helical creeping-wave pulse (3).

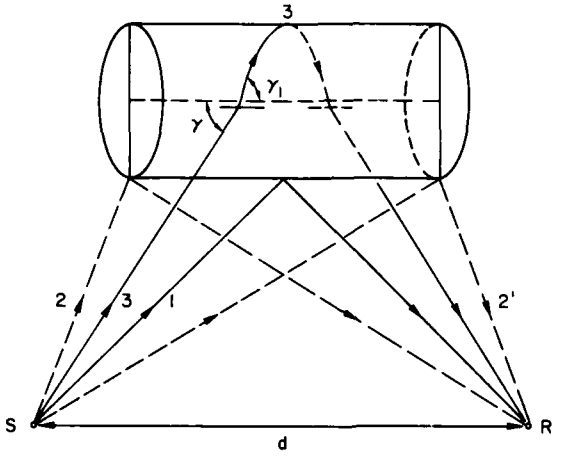

Fig. 11. Geometry of radar pulse scattering experiment observing helical creeping waves (3) on a conducting cylinder.

The reflected pulse shapes are close replicas of the incident pulse, with partially calculable distortions [24]. The creeping wave pulse, however, is distorted due to the dispersion contained in (16c). Its amplitude, after having traveled a distance $s = (a^2\theta^2 + z^2)^{1/2}$ over the cylinder surface, is given by

$$p_{\text{creep}}(s, t) = \int_{-\infty}^{\infty} G(\omega) \exp i\omega\left(\frac{s}{c_l} - t\right) d\omega \tag{24b}$$

where to lowest order, c_l may be taken from (16c) since TE creeping waves on conducting cylinders and acoustic creeping waves on rigid cylinders have the same phase velocity, to this order [39] (including the value of q_l). It turned out, however, that due to the width of $G(\omega)$, a more accurate representation was needed. Accordingly, a five-term representation of $\hat{n}_l$ for the cylinder, analogous to (16b), was used as given by Franz and Galle [39].

Figure 12 shows the measured signal vs. time corresponding to the experiment of Fig. 11, after subtraction of

(i) instrumental clutter (measured without target),
(ii) the specularly reflected pulse, and
(iii) the edge-diffracted pulses.

While the distortion of (ii) could be taken into account accurately [24], (iii) is a hard to calculate for a curved edge and we subtracted a replica of the incident pulse instead, resulting in an incomplete subtraction

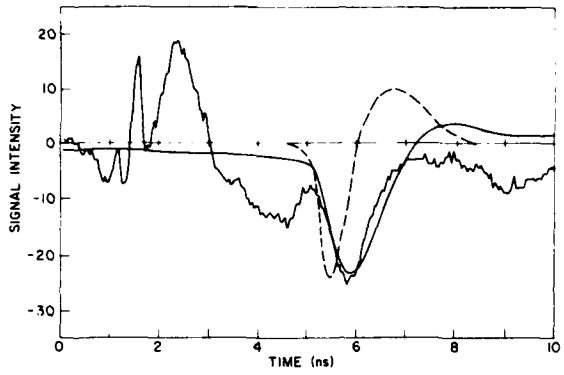

Fig. 12. Experimental helical creeping-wave pulse on a conducting cylinder, compared with calculated dispersive (solid curve) and non-dispersive (broken curve) creeping wave pulses.

in the region of 1–5 ns after the specular arrival (the original height of the latter amplitude was ~80 on the scale of Fig. 12).

Overlaid on the figure is the creeping wave calculated from (24b) (solid curve), as well as an artificial creeping wave calculated assuming no dispersion (dashed curve), which is thus an exact replica of the incident pulse. The agreement with the observed creeping pulse is striking, in view of the fact that no free parameters entered the calculation. The agreement thus includes the arrival time, polarity, amplitude, and dispersion of the creeping waves. Similar calculations were carried out for the sphere, and also for upright cylinders (TM modes). Due to the higher attenuation of these modes, no creeping waves could be observed in the latter case, however.

7. Resonance scattering from targets of arbitrary shape: Acoustic case

While the above-discussed examples treated analytically the scattering resonances in targets of separable geometry, bodies of arbitrary (non-separable) shape are obviously of very great importance. Field expansions in spherical coordinates, such as (1a, b), (12) or (14a), can still be used for this, but the non-separable shape of the target will induce a coupling of the channels, i.e. the nth normal mode of the incident wave will be coupled to all normal modes of the scattered wave, and vice versa. The T-function T_n of (14), e.g., will thus be replaced by a 'T matrix'. The corresponding T matrix method was introduced by Waterman [40] (see also Pao [41]), and we shall use it as a basis of our further discussion.

The T-matrix method has been combined by us with the resonance approach in the acoustic case [42]. Originally, Waterman had also applied his T-matrix approach to radar scattering from conducting bodies [43], and we have adapted his computer program, which originally was designed for the calculation of scattering amplitudes only, to the task of obtaining the complex-frequency (SEM) poles of the scattering amplitudes for conductors of arbitrary shape [44].

Examples of spheroids and finite-length cylinders have been treated in this way, and we have furthermore generalized Waterman's scattering code which was originally restricted to the case of axially-symmetric bodies [43], to targets of nonaxial shape so that the SEM poles of ellipsoidal targets could be obtained also [44].

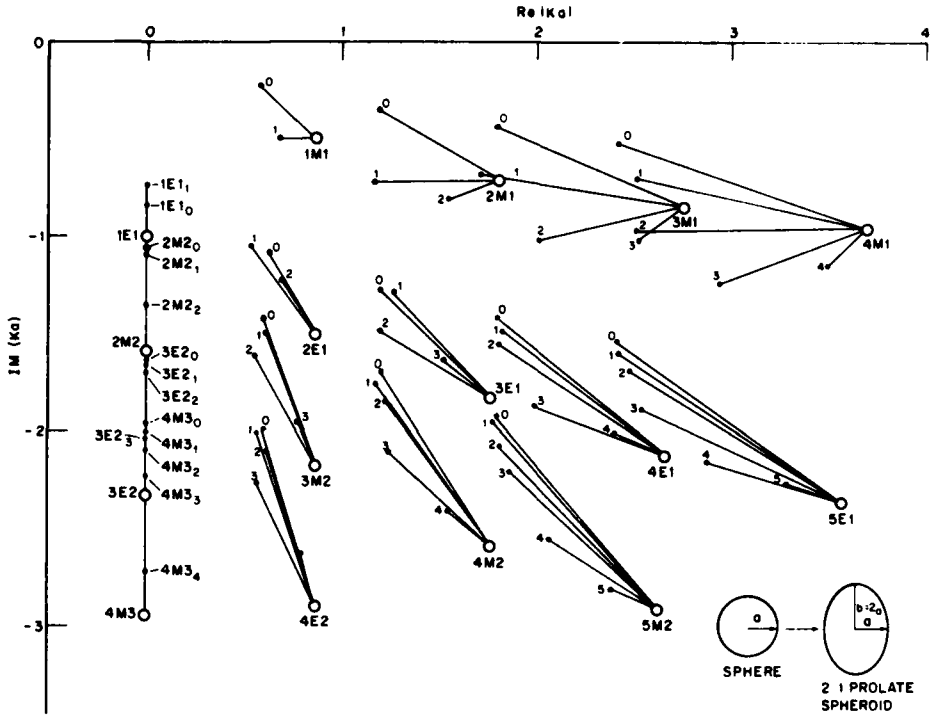

Fig. 13. Shifts and splittings of SEM poles in the complex frequency plane upon deformation of a conducting sphere into a 2:1 prolate spheroid (from [23, 44]).

The following two figures present some of our results on these topics. Figure 13 plots the (external) TM poles of a conducting sphere, identical to those in Fig. 9, as large circles labeled by (nMl), as well as TE poles labeled by (nEl), and shows how they shift and split as the sphere is deformed into a 2:1 spheroid by stretching the axis of symmetry (b), while the short axes are kept equal to a. The split components are labeled by an azimuthal quantum number m. Previous work [7] had only obtained the $m = 0$ components and their shifts, but had ignored the splitting of the poles into various m components.

A different way of presenting these results can be taken by plotting the real parts of the pole frequencies only, in the form of a 'level digram' familiar from atomic physics. This is done in Fig. 14, and it seems proper calling this approach '*Radar Spectroscopy*' [23], in analogy to optical spectroscopy which is based on atomic level diagrams. Figure 14 shows the $(nEl)_m$ spectra, for $l = 1$ (the least-damped) creeping-wave poles only, successively for a conducting sphere, a 1:1 cylinder, a 2:1 spheroid, a 2:1 cylinder and a very long (100:1) cylinder, the latter taken from [7]. The point of such a radar spectral diagram is that it indicates the sensitivity of the levels to changes in shape of target, hence offering the possibility of target identification and the determination of *target shape* from an experimentally obtained resonance spectrum of the target. This point will be elaborated on below.

8. Acoustic spectroscopy: The inverse problem

An 'acoustical spectrogram' similar to that of Fig. 14 has been obtained by us for the acoustical case [22], and is shown in Fig. 15. It presents the (internal) real, normalized eigenfrequencies $x = \omega a/c$ of fluid objects in vacuum (which is a good approximation for, e.g., water drops in air), and shows the level

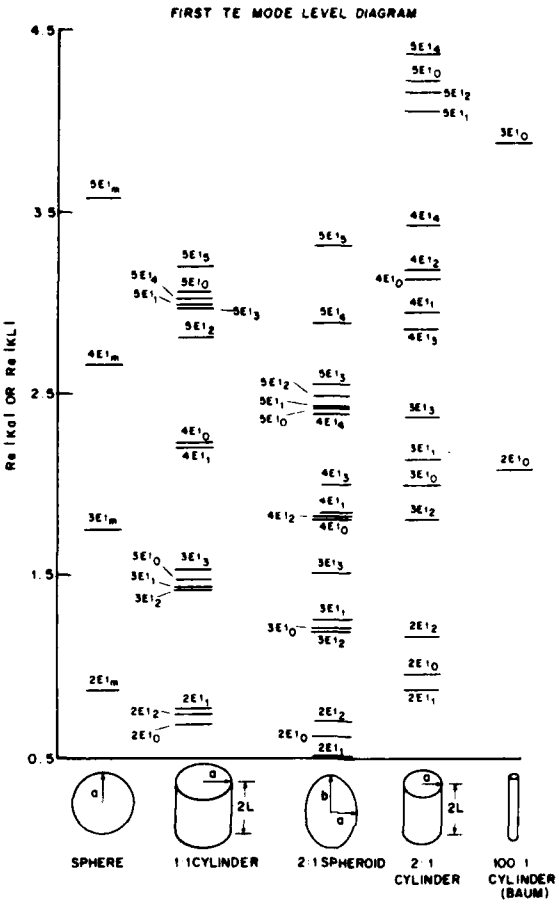

Fig. 14. 'Radar Spectroscopy' diagram of the real parts of SEM pole positions of a conducting sphere, 1:1 cylinder, 2:1 spheroid, 2:1 cylinder, and 100:1 cylinder ($l = 1$ TE poles only), showing level shifts and splittings (from [23]).

shifts and splittings as the sphere is deformed into a $b/a = 1.11\ldots:1$ prolate spheroid or circular cylinder, a 4:1 spheroid and cylinder, and finally an infinite cylinder. The levels are degenerate with respect to azimuthal quantum number m for the sphere, then split up, but become degenerate again with respect to the axial quantum number, for the infinite cylinder.

These eigenfrequencies were here determined by us not via a use of the T-matrix method, but by searching for the zeros in frequency of radial spheroid eigenfunctions on the boundary; the internal cylinder problem, however, is soluble in an elementary fashion.

If experimentally, a sufficient portion of the eigenfrequency spectrum of the target has been determined e.g. from an analysis of the scattered echoes, an attempt at target classification (i.e., solution of the inverse problem), can be made. For the sphere, the eigenfrequencies are determined from the zeros of the spherical Bessel functions, and if the measured spectral level ratios agree with the Bessel function zeros, the spherical nature of the target is established. The absolute value of any eigenfrequency then provides us with the ratio a/c where c is the sound speed inside the target. If the spectrum shows the sequence of spheroidal levels, the spheroidal nature of the target is established and the ratios a/c and b/c can be determined by absolute level measurements.

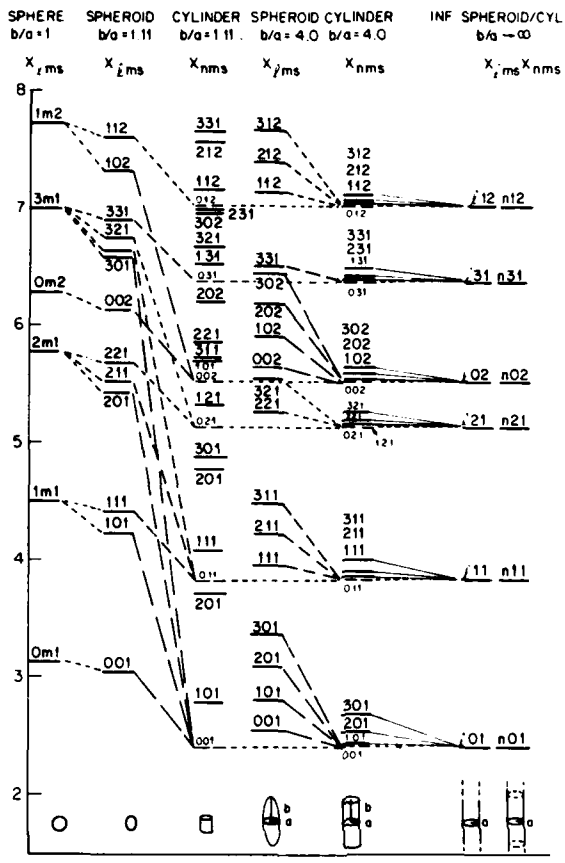

Fig. 15. 'Acoustical Spectroscopy' diagram for the eigenfrequencies of fluid objects in vacuum: sphere, prolate spheroids, finite and infinite cylinders, showing level shifts and splittings (from [22]).

An experimental determination of the eigenfrequency spectrum of an elastic cylinder by acoustic scattering has recently been accomplished by Maze, Taconet and Ripoche [45] in an ingenious fashion. If a conventional tone-burst (near-steady state) experiment is performed, the amplitude measured at various frequencies consist of an interfering superposition of resonances and background in the fashion of (7d), from which the resonances are often hard to separate, due to the fact that the measured data show all resonances contained in the sum over modes n. Part (b) of Fig. 16 presents such a measured spectrum consisting of resonances and background, for the case of an aluminum cylinder in water. If, however, one waits until the specularly reflected background has passed, the slightly attenuated Whispering-Gallery waves which keep circulating around the cylinder in a resonant fashion, will then provide an echo signal that, upon a frequency sweep, shows their resonance spectrum (part (a) of Fig. 16). This procedure represents a direct experimental way of determining the pure acoustic spectral diagram of a target, without the interference of a reflected-wave or external resonant background, hence offering a direct approach to acoustic spectroscopy and target classification. Indeed, part (c) of Fig. 16 shows the calculated (top) and measured (bottom) resonance frequencies of the cylinder, labeled by n (mode number) and l (surface wave label). Such a comparison offers the possibility of a determination of the

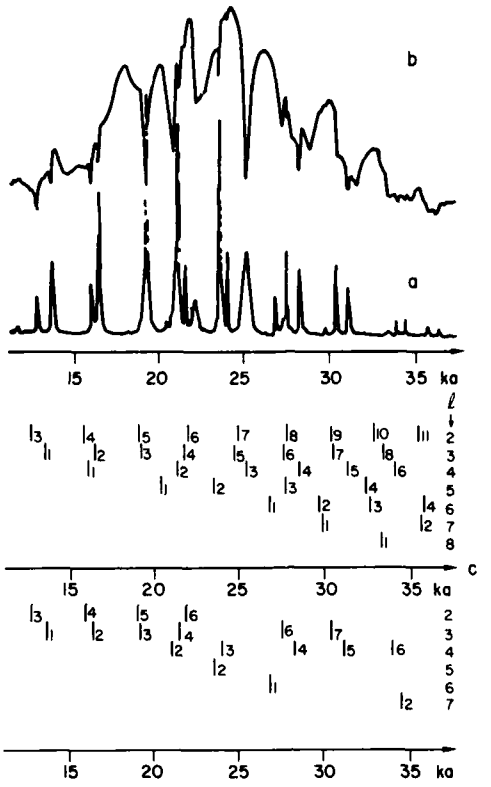

Fig. 16. Measured acoustic spectrum of an aluminum cylinder in water, (a) pure resonances, (b) resonances and background, (c) comparison of measured and calculated resonance frequencies (from [45]).

material composition of the target via acoustic spectroscopy, just as optical spectroscopy determines the chemical composition of a substance. The term 'Acoustic Spectroscopy' has been coined in this connection by Derem [46].

9. Summary

The preceding examples illustrate the accomplishments of the Resonance Scattering Theory [1] in a great variety of fields of classical physics (radar, sonar, elastic waves and geophysics) regarding two principal aspects, namely:

(i) providing analytical connections between the resonances of a target (the 'SEM poles') and the (internal and external) surface waves on the target (described by 'Regge poles'), and hence establishing a physical interpretation of the resonances, and

(ii) providing a potential means for the solution of the inverse scattering problem, i.e. the identification, and the material and shape determination of the target from an analysis of the resonance effects contained in the returned echo signals.

In relation to the inverse problem, we have here proposed to represent the spectrum of resonance frequencies of a given target by a 'level scheme' similar to that of atomic spectra, and have accordingly

termed this approach '*Radar Spectroscopy*' or '*Acoustic Spectroscopy*' (see also [46]). The shifting and splitting of the levels during the changes of shape of a target of known composition (and, by implication, the analogous level shifts undergone during changes of composition) which we have illustrated here, then offer a possibility for target identification, and hence for a solution of the inverse problem. Some experience will be required when putting such a scheme into working order, as it has been the case in optical spectroscopy as well. In addition to merely the level positions and their widths, the *intensities* of the resonance excitations (i.e., the SEM pole residues) will provide crucial information on these and on other aspects of the inverse problem such as target orientation, as will the use of polarization data. (Note that level positions and resonance widths are inherent properties of a target while their excitation strengths depend on the means of excitation chosen, such as the incident beam direction and polarization with respect to the target geometry.)

From the foregoing discussion, there emerges a global picture of target resonance effects that promises to result in a useful tool for target identification and for a solution of the inverse problem. The mentioned recent experimental work [45], which has provided a way of exhibiting the pure scattering resonances in a direct fashion for the acoustic case, should be particularly relevant in this respect.

Acknowledgment

The Catholic University personnel acknowledges the support of the Naval Air Systems Command, AIR-310B, regarding the electromagnetic studies reported here, and of the Office of Naval Research regarding the Acoustics aspects. The Naval Surface Weapons Center personnel acknowledges support by the Center's Independent Research Board. D. Brill received the support of Code 2842 of David Taylor Naval Ship Research and Development Center, and the University of Puerto Rico (Mayaguez) personnel was supported by Grant No. DAAG29-81-G0016 of the US Army Research Office.

References

[1] L. Flax, G.C. Gaunaurd and H. Überall, 'Theory of resonance scattering', in: W. P. Mason and R. N. Thurston, Eds., *Physical Acoustics Vol. 15*, Academic Press, New York (1980) 191–294.
[2] D. Brill, G. C. Gaunaurd and H. Überall, 'The response surface in elastic wave scattering', *J. Appl. Phys. 52*, 3205–3214 (1981).
[3] A. Sommerfeld, *Partial Differential Equations in Physics*, Academic Press, New York (1949).
[4] R.G. Newton, *The Complex j-Plane*, Benjamin, New York (1964).
[5] W. Franz, *Theorie der Beugung elektromagnetischer Wellen*, Springer, Berlin (1957).
[6] J.M. Blatt and V.F. Weisskopf, *Theoretical Nuclear Physics*, Wiley, New York (1952).
[7] C.E. Baum, 'The singularity expansion method', in: L.B. Felsen, Ed., *Transient Electromagnetic Fields*, Springer, Berlin (1976) 130–179.
[8] H. Überall and G.C. Gaunaurd, 'The physical content of the singularity exapnsion method', *Appl. Phys. Lett. 39*, 362–364 (1981).
[9] G.C. Gaunaurd, H. Überall and A. Nagl, 'Complex frequency poles and creeping-wave transients in electromagnetic-wave scattering', *Proc. IEEE, 71*, 172–174 (1983).
[10] H. Überall and G.C. Gaunaurd, 'Acoustic surface wave pulses and the ringing of resonances', *J. Acoust. Soc. Amer. 72*, 1014–1017 (1982).
[11] W.M. Boerner, A.K. Jordan and I.W. Kay, Eds., *IEEE Trans. Antennas and Propagation 29* (1981), Special Issue on Inverse Methods in Electromagnetics.
[12] P.C. Sabatier, Ed., *Applied Inverse Problems*, Springer, Berlin (1978).
[13] K. Chadan and P.C. Sabatier, *Inverse Problems in Quantum Scattering Theory*, Springer, Heidelberg (1977).
[14] G.C. Gaunaurd and H. Überall, 'Deciphering the scattering code contained in the resonance echoes from fluid-filled cavities in solids', *Science 206*, 61–64 (1979).
[15] G.C. Gaunaurd and H. Überall, 'Identification of cavity fillers in elastic solids using the resonance scatttering theory', *Ultrasonics 18*, 261–269 (1980).

[16] G.C. Gaunaurd and H. Überall, 'Electromagnetic spectral determination of the material composition of penetrable radar targets', *Nature 287*, 708–709 (1980).
[17] G.C. Gaunaurd, H. Überall and P. J. Moser, 'Resonances of dielectrically coated conducting spheres and the inverse scattering problem', *J. Appl. Phys. 52*, 35–43 (1981).
[18] G.C. Gaunaurd and H. Überall, 'Solution of the inverse scattering problem in the resonance case', *IEEE Trans. Antennas and Propagation 29*, 293–297 (1981).
[19] R. Fiorito and H. Überall, 'Resonance theory of acoustic reflection and transmission through a fluid layer', *J. Acoust. Soc. Amer. 65*, 9–14 (1979).
[20] R. Fiorito, W. Madigosky and H. Überall, 'Resonance theory of acoustic waves interacting with an elastic plate', *J. Acoust. Soc. Amer. 66*, 1857–1866 (1979).
[21] R. Fiorito, W. Madigosky and H. Überall, 'Acoustic resonances and the determination of the material parameters of a viscous fluid layer', *J. Acoust. Soc. Amer. 69*, 897–903 (1981).
[22] D. Brill, G.C. Gaunaurd and H. Überall, 'Acoustic spectroscopy', *J. Acoust. Soc. Amer. 72*, 1067–1069 (1982).
[23] P.J. Moser and H. Überall, 'Radar spectroscopy: T-matrix approach', *Proc. Internat. IEEE/AP-S Symposium and National Radio Science Meeting*, p. 50, June 16–19, 1981, Los Angeles, CA, and *Proc. IEEE 71*, 171–172 (1983).
[24] G.T. Ruck et al, *Radar Cross Section Handbook*, Plenum, New York (1970).
[25] P.J. Moser, J.D. Murphy, A. Nagl and H. Überall, 'Resonances and surface waves on conducting spheres with a dielectric coating', *Radio Sci. 16*, 279–288 (1981).
[26] P.J. Moser, J.D. Murphy, A. Nagl and H. Überall, 'Creeping-wave excitation of the eigenvibrations of dielectric resonators', *Wave Motion 3*, 283–295 (1981).
[27] G. Bollig and K. Langenberg, 'Ultrasonic defect classification', presented at DARPA/AF Meeting: *Review of Progress in Quantitative Nondestructive Evaluation*, August 2–7, 1981, Boulder, CO.
[28] J.D. Murphy, P.J. Moser, A. Nagl and H. Überall, 'A surface wave interpretation for the resonances of a dielectric sphere', *IEEE Trans. Antennas and Propagation 28*, 924–927 (1980).
[29] G.C. Gaunaurd and H. Überall, 'Numerical evaluation of modal resonances in the echoes of compressional waves scattered from fluid-filled spherical cavities in solids', *J. Appl. Phys. 50*, 4642–4660 (1979).
[30] G.C. Gaunaurd and H. Überall, 'RST analysis of monostatic and bistatic acoustic echoes from an elastic sphere', *J. Acoust. Soc. Amer. 73*, 1 (1983).
[31] A. Nagl, H. Überall, P.P. Delsanto, J.D. Alemar and E. Rosario, 'Refraction effects in the generation of helical surface waves on a cylindrical obstacle', *Wave Motion 5*, 235–247 (1983).
[32] H. Takeuchi and M. Saito, 'Seismic surface waves', in: B.A. Bolt, Ed., *Methods in Computational Physics Vol. 11*, Academic Press, New York (1972) 217–295.
[33] F. Gilbert and A.M. Dziewonski, 'An application of normal mode theory to the retrieval of structural parameters and source mechanisms from seismic spectra', *Philos. Trans. Roy. Soc. London Ser. A 278*, 187–269 (1975).
[34] G. Igiri and H. Überall, 'Surface waves on a radically stratified earth', *IEEE Trans. Geosci. Remote Sensing*, to appear.
[35] M. Landisman, T. Usami, Y. Satô and R. Massé, 'Contribution of theoretical seismograms to the study of modes, rays, and the earth', *Rev. Geophys. Space Phys. 8*, 533–589 (1970).
[36] E. Heyman and L.B. Felsen, 'Creeping waves and resonances in transient scattering by smooth convex objects', preprint.
[37] G.C. Gaunaurd, J.V. Subrahmanyam and H. Überall, 'Relation between the ringing of resonances and surface waves in radar scattering', preprint.
[38] H. Überall, A. Nagl, J.V. Subrahmanyam, B.Z. Hollmann, G.C. Gaunaurd and J.D. Murphy, 'Physical basis of the singularity expension method in terms of creeping waves (theory and experiment)', *Proc. Internat. IEEE/AP-S Symposium and National Radio Science Meeting*, p. 71, June 16–19, 1981, Los Angeles, CA.
[39] W. Franz and R. Galle, 'Semiasymptotische Reihen für die Beugung einer ebenene Welle am Zylinder', *Z. Naturforsch. A 10*, 374–378 (1955).
[40] P.C. Waterman, 'New formulation of acoustic scattering', *J. Acoust. Soc. Amer. 45*, 1417–1429 (1969).
[41] Y.H. Pao, 'The transition matrix for the scattering of acoustic waves and for elastic waves', in: J. Miklowitz and J.D. Achenbach, Eds., *Modern Problems in Elastic Wave Propagation*, Wiley-Interscience, New York (1978) 123–144.
[42] H. Überall, G.C. Gaunaurd and E. Tanglis, 'Interior and exterior resonances in acoustic scattering II', Department of Physics, Catholic University, Report (1981) and *Nuovo Cimento B*, to appear.
[43] P.C. Waterman, 'Numerical solution of electromagnetic scattering problems', in: R. Mittra, Ed., *Computer Techniques for Electromagnetics*, Oxford (1973).
[44] P.J. Moser, 'The isolation, identification and interpretation of resonances in the radar scattering cross section of conducting bodies of finite general shape', Ph.D. Thesis, Department of Physics, Catholic University of America, Washington, DC (1982).
[45] G. Maze, B. Taconet and J. Ripoche, 'Influence des ondes de "galerie à echo" sur la diffusion d'une onde ultrasonore plane par un cylindre', *Phys. Lett. A 84*, 309–312 (1981).
[46] A. Derem, 'Relation entre la formation des ondes de surface et l'apparition de résonances dans la diffusion acoustique', *Rev. Cethedec 58*, 43–79 (1979).